Atmos. Chem. Phys. Discuss., 9, 6827–6854, 2009
www.atmos-chem-phys-discuss.net/9/6827/2009/

Atmospheric Chemistry and Physics Discussions

This discussion paper is/has been under review for the journal *Atmospheric Chemistry and Physics (ACP)*. Please refer to the corresponding final paper in *ACP* if available.

Vertical distribution of aerosols in Mexico City during MILAGRO-2006 campaign

P. A. Lewandowski[1], **W. E. Eichinger**[1], **H. Holder**[2], **and J. Prueger**[3]

[1]IIHR-Hydroscience & Engineering, University of Iowa, Iowa City, Iowa 52242, USA
[2]Duke University, Rayleigh, NC, USA
[3]National Soil Tilth Laboratory, Ames, IA, USA

Received: 8 February 2009 – Accepted: 18 February 2009 – Published: 11 March 2009

Correspondence to: P. A. Lewandowski (piotr-lewandowski@uiowa.edu)

Published by Copernicus Publications on behalf of the European Geosciences Union.

Abstract

On 7 March 2006, a mobile, ground-based, vertical pointing, elastic lidar system made a North-South transect through the Mexico City basin. Aerosol size distribution measurements, made concurrently, allowed calculation of the mass extinction efficiency (MEE) for the lidar system (1064 nm). MEE combined with an inverted lidar extinction coefficient resulted in total aerosol vertical mass estimates with 1.5 m vertical spatial and 1 s temporal resolution.

The results showed that the aerosol loading within the basin is about twice what is observed outside of the basin. The total aerosol base concentrations observed in the basin are of the order of 200 $\mu g/m^3$ and the base levels outside are of the order of 100 $\mu g/m^3$. The local heavy traffic events can introduce aerosol levels near the ground as high as 900 $\mu g/m^3$. The lidar-based total aerosol loading compares with the hourly-averaged PM_{10} ground observations conducted by the RAMA monitoring network throughout Mexico City.

1 Introduction

Mexico City Metropolitan Area (MCMA) is one of the largest and fastest growing populated areas in the world. With a population close to 20 million people and over 4 million vehicles, it is also the largest source of anthropogenic pollution in the region (CAM, 2002, 2006). Its elevated location (~2200 m) and tropical climate facilitate photolysis and transport of urban and industrial pollutants on a continuum of scales, from local, through regional, to continental. The chemical properties of MCMA pollutants have been analyzed in the past, e.g. MCMA-2003 campaign (Molina et al., 2007). The key results from the MCMA-2003 campaign formed the basis for yet more extensive atmospheric measurement campaign MILAGRO/MIRAGE/MCMA2006/INTEX-B, which was conducted in March 2006 in Mexico (Molina et al., 2008). Numerous chemistry studies have been carried out during the MILAGRO campaign (e.g. Stephens et al., 2008;

ACPD

9, 6827–6854, 2009

Adachi and Buseck, 2008; Thornhill et al., 2008; DeCarlo et al., 2008; Nunnermacker et al., 2008; Kleinman et al., 2008; Talbot et al., 2008; Shon et al., 2008; Zheng et al., 2008; Doran et al., 2008). These studies revealed the significance of primary and secondary aerosols in the context of pollutant chemistry and air quality.

Physical properties of aerosols were also of great importance during the MILAGRO campaign in 2006. Spatial and temporal measurements of aerosol distribution in Mexico City region were intended to provide information on transport, dynamics and evolution of particles aloft. Each component of the campaign was carried out on a different spatial scale, from urban pollution supported by ground-based point measurements, to regional large scale pollution transport supported by wide-coverage aircraft measurements. The goal of the multiscale approach in the MILAGRO campaign was to bridge various points of the continuum to better understand the environmental impacts of pollution sources, such as MCMA. For that purpose several profilers, radiosondes and lidars (airborne, ground stationary and ground mobile) were dedicated to measuring the vertical layering of aerosols on different scales (Shaw et al., 2007).

Lidars are particularly suitable for measuring physical properties of small particles. They capture spatio-temporal distribution and mechanical mixing of particles suspended in the air (Eichinger et al., 2008a, b; Kao et al., 2002; Holmen et al., 1998) as well as mark the planetary boundary layer (PBL) height (Cooper et al., 2006; Eichinger et al., 2005; Cooper and Eichinger, 1994).

The University of Iowa mobile, ground-based, upward-looking lidar was used to support vertical measurements of aerosols on local and regional scales during the MILAGRO campaign. The 1064 nm lidar system was mounted on a flatbed truck and was able to make vertical measurements while in motion (Fig. 1). The lidar data was supported by solar transmittance data, measured with an optical sun photometer. The solar photometer measured direct and indirect (almucantar) radiation once every 1–2 h. These measurements enabled calculation of aerosol size distribution (ASD) data (Nakajima et al., 1996). Due to the nature of the measurements (the propagating medium was the entire atmosphere), the ASD obtained from these measurements rep-

ACPD
9, 6827–6854, 2009

resents an average aerosol size distribution in the atmospheric column.

On 7 March 2006, in the presence of light, northerly winds (de Foy et al., 2008; Fast et al., 2007), the University of Iowa mobile vertical lidar system performed a North-South transect through the Mexico City basin. The lidar system measured vertical and horizontal distribution of the various aerosol layers. The unique topography of the basin created conditions in which the northerly winds were venting the valley, mostly through a narrow pass in the South of the basin. The measurements on 7 March were intended to capture the venting of the basin through the pass and observe the transition between inside and outside of the valley. The exact route is illustrated in Fig. 2.

From the electromagnetic point of view, extinction efficiency is a measure of the amount of energy removed by a particle from a wave by means of scattering and absorption. Depending on the size of the particle, refractive index and the wavelength of an incident radiation, Rayleigh and Mie theories report the exact values of the extinction efficiencies (such as the function presented in Fig. 3). Taking particles of all sizes from a participating medium and combining them with the corresponding extinction efficiencies, multiplied by their cross sectional areas, will result in the extinction coefficient. The extinction coefficient is a macroscopic quantity that describes the amount of energy removed from an electromagnetic wave per unit distance for any given wavelength. Lidar measurements can provide spatially resolved extinction coefficient data for a certain wavelength (Klett, 1981, 1985; Kovalev, 2003; Kovalev and Eichinger, 2004). Using the extinction coefficient data from the lidar and aerosol size distribution data from the sun photometer, one can invert the problem and determine the number (or mass) of particles in the medium.

Extinction efficiency for 1064 nm implied from Mie theory (Fig. 3) is combined with column averaged ASD obtained from the sun photometer (Fig. 4b), resulting in a quantity called the Mass Extinction Efficiency (MEE). The MEE is a ratio of the total column extinction coefficient at the wavelength of the lidar, to the total mass concentration of aerosol in the column (Eq. 4). In electromagnetic sense, the MEE is a measure of the amount of energy removed from the wave by a specific aerosol (characterized by ASD)

ACPD
9, 6827–6854, 2009

per unit length per unit concentration of the aerosol.

The MEE approach allows estimation of the absolute aerosol mass concentration (Eq. 5) with the resolution of lidar (1.5 m spatial and 1 s temporal). This method is unique and introduces new data-rich capabilities to the aerosol research community. Due to the large spatial extent of the data, it is rather difficult to validate the MEE-derived results by means of in-situ measurements. Yet the effort of validating this method with ground-based PM_{10} network in Mexico City is also presented in the results section.

2 Instruments

2.1 Lidar

Lidar operates by emitting a pulse of laser light into the atmosphere. Particulates interact with the pulse and scatter light back to the lidar. The term "elastic" refers to scattering in which no energy is lost by the photons, so that the detected light is at the same wavelength as the emitted light.

For the purpose of the study, the University of Iowa lidar (Eichinger et al., 1999) was retrofitted into a mobile laboratory mounted on the bed of a truck (Fig. 1). The lidar operated continuously while the truck was in motion, simultaneously recording the GPS position of the instrument.

A Nd:YAG laser operating at the 1064 nm wavelength provided the light source. The laser was attached to a 0.25 m, $f/10$, Cassegrain telescope. The laser pulsed at 50 Hz with ~25 mJ energy per pulse. The laser beam was emitted co-axial with the telescope. The backscattered signal was measured by an IR-enhanced Si-APD detector and then digitized by a 100 MHz digitizer. The resulting spatial (vertical) resolution was 1.5 m. The maximum useful range was 3400 m. For improved data accuracy, the signals from 50 pulses were averaged to 1 s profiles.

ACPD
9, 6827–6854, 2009

2.2 Sun photometer

A commercial, fully automated Prede POM-01L sun photometer was used for this study. It was a 7 wavelength system with 315, 400, 500, 675, 870, 940 and 1020 nm filters operated by a filter wheel. The half-angle view of the instrument was 1 degree and the half-power bandwidth was 10 nm (with the exception of 3 nm for 315 nm). The instrument was mounted on top of the mobile laboratory only for the time of the measurement and taken down during travel.

The instrument measured the relative radiation intensities (direct and almucantar) and was calibrated using a standard Langley method (Holben et al., 1998). The direct solar measurements provided total optical depth estimate and the almucantar measurements data were processed for aerosol size distribution using SKYRAD.pack v.4.2 (Nakajima et al., 1996).

2.3 Ground PM_{10} measurements

The ground PM_{10} measurements were conducted by the Mexican government scientists within the RAMA network (Red Automática de Monitoreo Atmosférico). The network included 16 sites located throughout Mexico City that had PM_{10} capability. Figure 2 shows the locations of the 6 RAMA sites nearest to the lidar route.

3 Data analysis

3.1 Lidar inversion method

Elastic lidar cannot measure extinction coefficients directly. Instead, it measures a relative backscattered power $P(r)$ which can be inverted to estimate extinction. Equa-

tion (1) is the range corrected lidar equation (Kovalev and Eichinger, 2004)

$$P(R)R^2 = C_0\beta(R)\exp\left(-2\int_0^R \alpha(R')dR'\right), \quad (1)$$

where R is the distance from the lidar to a given sampling volume, β is the backscatter coefficient, α is the extinction coefficient, $C_0{=}P_0Ac\tau/2$ is the lidar constant, A is the telescope aperture area, τ is the laser pulse length, c is the velocity of light and P_0 is the power transmitted by the laser. In order to invert the lidar equation, the extinction and backscatter coefficients are assumed to be related by a power law (Klett, 1981, 1985)

$$\beta(R) = B_0\alpha^k(R), \quad (2)$$

where k is a constant power and B_0 is a scaling factor (often called the lidar ratio if $k{=}1$). With the assumption from Eq. (2), one can now estimate the extinction using the Klett method (Klett, 1981, 1985)

$$\alpha(R) = \frac{\exp[(S - S_0)/k]}{\left\{\frac{1}{\alpha_0} - \frac{2}{k}\int_{R_0}^R \exp[(S - S_0)/k]dR'\right\}} \left[\frac{1}{\text{km}}\right], \quad (3)$$

where $S{=}\ln[P(R)R^2]$. While there are other more complex algorithms for calculating extinction (Kovalev and Eichinger, 2004), the Klett method is fully adequate approach for the purpose of this study.

3.2 Aerosol mass concentration

The knowledge of aerosol size distribution (ASD) is useful in combination with lidar data. It allows for estimating the absolute aerosol mass loading in the atmosphere. Studies show that the extinction (e.g. estimated from the lidar returns) is highly correlated with PM_{10} aerosol concentrations (Del Gusta and Marini, 2000; Lagrosas et al.,

ACPD
9, 6827–6854, 2009

2005). The quantity that combines extinction and mass is commonly called Mass Extinction Efficiency (MEE). It is a ratio of total extinction in the column to the total column mass concentration of aerosols for any given ASD and any given wavelength. MEE links extinction efficiency derived from the Mie theory with aerosol mass estimates and in conjunction with lidar can provide high spatial resolution aerosol mass estimates.

The total extinction is simply a product of Mie extinction efficiency, the particle cross sectional area and the number of particles of each size integrated over all particle sizes for a given wavelength (the numerator in Eq. 4). The total mass of aerosol is a product of the particle volume, the mass density of particle and the number of particles, integrated over all sizes (the denominator in Eq. 4). Equation (4) presents MEE in the following form (Lagrosas et al., 2005)

$$\mathrm{MEE} = \frac{\pi \int_{r_1}^{r_2} r^2 Q_{\mathrm{ext}}(r,\lambda,m) n(r) dr}{\frac{4}{3}\pi\rho \int_{r_1}^{r_2} r^3 n(r) dr} \quad \left[\frac{1/\mathrm{m}}{\mathrm{g/m^3}}\right], \tag{4}$$

where r is the particle size, r_1 and r_2 are ASD limits, Q_{ext} is Mie extinction efficiency calculated for the 1064 nm wavelength (Fig. 3), m is the assumed refractive index of the aerosol, $n(r)$ is a given ASD (Fig. 4b) and ρ is the particle density. Using the extinction estimated from the lidar data, one can obtain the aerosol mass concentration with the resolution of the lidar measurements

$$C(R) = \frac{\alpha(R)}{\mathrm{MEE}} \quad \left[\frac{\mathrm{g}}{\mathrm{m^3}}\right], \tag{5}$$

where α and MEE have been previously defined. The entire data processing flow leading to Eq. (5) is shown in Fig. 5.

ACPD
9, 6827–6854, 2009

4 Results and discussion

4.1 Aerosol size distribution

During the transect, 16 sun photometer measurements were taken in and outside the basin, in 3 discrete series (Fig. 4a). The data from the measurements were used to estimate a column averaged aerosol size distribution (ASD) with SKYRAD.pack.v.4.2 software[1] (Nakajima et al., 1996). The resulting ASD estimates are presented in Fig. 4b.

The measurements within each of the 3 sets of data in Fig. 4a are nearly identical with little deviation. Although the differences in raw data were small, they propagated into noticeable deviations in the respective size distributions, total volume of aerosols and MEE values (Fig. 4b).

Of all the 3 sets of raw data (Fig. 4a), the earliest measurement (~9 a.m.) has the largest number of measured scattering angles due to the lowest sun elevation angle. This enabled better convergence of the inversion software and thus the earliest measurements show the least uncertainty in the ASD shape, total volume and MEE value.

Despite the uncertainties, all of the 3 sets of the size distributions are similar in shape, which implies that the dominant source of particles is common to all the measurements. The spectra are bimodal with the fine mode being most likely anthropogenic in origin (peaks at around 0.2 µm) and the coarse mode being the biogenic pollution, primarily windblown dust (peaks at around 7–8 µm).

4.2 MEE results

MEE is extremely sensitive to the shape of the ASD function. This poses a big challenge in quantifying the MEE as the ASD is often spatially and temporally dynamic. Despite this, the literature reports MEE values ranging from 1.2 $m^2\,g^{-1}$ (coarse particles

[1] Available at http://www.ccsr.u-tokyo.ac.jp/~clastr/

ACPD
9, 6827–6854, 2009

dominant) to 12 $m^2\,g^{-1}$ (fine particles dominant) (Husar and Falke, 1996; Di Girolamo et al., 1999; Lagrosas et al., 2005).

The MEE estimated from the ASDs in this study ranged from 0.5 $m^2\,g^{-1}$ to 1.3 $m^2\,g^{-1}$ (with the particle density, ρ, assumed 1 g/cm^3 for all the calculations). Higher values of MEE were observed inside the Mexico City basin whereas the lower values were observed outside of the basin. To maintain continuity in the mass concentration calculations using lidar data (Eq. 5), we assumed a constant ASD (and therefore a constant MEE) for the entire measurement period. This assumption is strong but it's also supported by similarly shaped ASD estimates within the basin (Fig. 4b). The earliest sun photometer measurement set 8:58 a.m.–9:07 a.m. was assumed constant and effective for the entire data analysis. Although the 8:58 a.m.–9:07 a.m. ASD data is the most consistent within the dataset, we admit the choice of the dataset is somewhat arbitrary. The corresponding value of MEE for the 8:58 a.m.–9:07 a.m. dataset was 0.9 $m^2\,g^{-1}$ and it was also constant during the entire analysis.

4.3 Transect through Mexico City

The transect through the Mexico City basin started at 6:18 a.m. on 7 March 2006 in the city of Pachuca, about 70 km NE of Mexico City (Fig. 2). The direction of the transect was north-to-south. The meteorological conditions reported for that day were favourable: persistent light northerly winds for the Mexico City basin, warm, mostly sunny, stable surface conditions in the morning (de Foy et al., 2008; Fast et al., 2007).

Figure 6b shows lidar-derived total aerosol concentration curtain corresponding to Fig. 2. Figure 6 additionally presents the total aerosol concentrations extracted from the lidar at 200 m above the ground (Fig. 6c) and the total optical depth for the 1064 nm wavelength (Fig. 6d).

At the beginning of the lidar measurements, at around 6:20 a.m., the aerosol curtain graph indicates a residual layer at approximately 4500 m a.s.l. with high concentration values decaying with time. This effect is due, at least in part, to water condensation

ACPD
9, 6827–6854, 2009

on the particulates. As the sun warms the air after dawn, decreasing the relative humidity and the water evaporates from the particulates, which decreases the apparent concentration values.

At around 6:30 a.m., only about 10 km south of the starting point, the Mexico City plume is found at about 200–300 m above the ground and as the lidar continues approaching the city, the plume is observed lower to the ground. At 7 a.m. the mobile lidar approached a dense traffic congestion on a major highway going through Mexico City (Fig. 6a indicates slow velocities from a traffic jam and Fig. 6b represents an abrupt increase in concentrations). This event resulted in an outburst of ground aerosol concentrations due to emissions from the congested traffic conditions (peaking at ~900 $\mu g/m^3$). While the concentration estimate seems to be extremely high, one should remember that this was an instantaneous measurement directly above a 6 lane highway. A high number of vehicles traveling on that road (diesel trucks and other petroleum vehicles with no or poor emission control) and the strength of the stable boundary layer at that early morning hour contributed to the sharp increase in particulate concentration. On top of the exhaust emissions, vehicles also tend to pick up a large amount of road dust and inject it directly into the boundary layer. It is not unusual to see similar structures localized over major thoroughfares in scanning lidar images (Cooper and Eichinger, 1994; Eichinger and Kraye, 1998). The surface structures observed during that time of day rose to about 1 km in height but did not reach nor mix with the upper residual layer. At around 7:30 a.m. the traffic congestion relaxed and the lidar proceeded further into the city. At this point, the height of pollution plume was observed to be at around 200–300 m above the ground with base concentrations of about 200 $\mu g/m^3$. This observation is confirmed by the RAMA network measurements, recording a similar average morning rush hour PM_{10} concentration level in the city (Fig. 8).

From about 7:30 a.m., another layer appears at around 3000 m a.s.l. (500 m above the ground). The layer is separated and at this point does not mix with the pollution from the ground. These conditions remained constant throughout the city until the southern

ACPD
9, 6827–6854, 2009

rim of the basin was reached at about 9:50 a.m. The southern outlet from the basin is elevated about 200 m with respect to the rest of the basin. This difference in elevation acts to keep the ground pollution from leaving the valley southbound (evident in lidar curtain plot in Fig. 6b).

Halfway through the pass (~10:25 a.m.), the vertical layering of the plume changed. The 3000 m a.s.l. layer disappeared while the 4500 m a.s.l. residual layer started to mix in with the rising boundary layer, which resulted in higher concentrations across the boundary layer and lower concentrations of around 100 $\mu g/m^3$ at the ground level.

Vertical mixing intensified at around 11 a.m. where local ground pollution was lofted as high as 1 km above the ground and entrained with the high altitude residual layer. At around 11:35 a.m. the lidar began the descent outside of the valley. The local ground pollution continued to grow in height but did not mix with the high level (4500 m a.s.l.) residual layer. Both structures were separated by a thin stable layer of relatively clean air. These conditions were maintained until the end of the transect at 12:25 p.m.

Figure 7 shows a histogram of the lidar-derived total aerosol concentration estimates for the inside (urban) and outside (rural) areas of the Mexico City basin. The rural concentrations (blue) show a narrow mode with a center located at around 110 $\mu g/m^3$. The urban concentrations are multimodal suggesting multiple contributors and pollution in the city. The values of the concentrations range from 150 $\mu g/m^3$ to 450 $\mu g/m^3$ with the most intensive mode at 300 $\mu g/m^3$.

Figure 9 presents the lidar data in 3-D display where each lidar profile is rendered with respect to its actual geographic location. The 3-D lidar data is overlaid onto a digital elevation model of the region using GIS software (ArcScene). Figure 9 is an example of a new approach to geospatial analysis of lidar data. It allows a better understanding the influence of a complicated topography on the vertical structures of planetary boundary layer.

ACPD
9, 6827–6854, 2009

4.4 Discussion on limitations of MEE approach

Each of the components in the analysis flowchart (Fig. 5) contains or introduces uncertainty. The complexity of the algorithms used in the analysis makes it difficult to quantify the resulting aerosol mass concentration uncertainty. For example while it is possible to quantify uncertainties related to the sun photometer measurements, it is difficult to quantify uncertainties related to the inversion algorithm itself. The inversion algorithm relies on the numerous assumptions (Nakajima et al., 1996) such as a known refractive index, proper calibration, sphericity of the particles, spatial and temporal homogeneity of the aerosol distribution, meteorological conditions, and the exact location of the instrument. Each of these factors is a potential source of additional inaccuracy. Mie theory, however accurate for spherical particles, only approximates real particle extinction efficiency and also introduces uncertainty.

Despite the amount of data provided by the measurements, lidar technology also has its own limitations. The fundamental limitation of using the lidar is "proper" data processing. The raw lidar data (the time series of the detector voltage) must be inverted into a physical quantity of interest, which in this case is the extinction coefficient. Although there are several methods of inverting the raw lidar data into extinction coefficients, none of these methods give an exact or unique solution. One must estimate the extinction based on strict assumptions, such as Eq. (2), which introduce uncertainty. The sources of uncertainties related with the lidar inversion have been extensively discussed in Kovalev and Eichinger (2004). The discrepancies can be seen in Fig. 6d, which shows the total optical depth from lidar (inverted using Eq. (3) and integrated over the whole lidar range) and the total optical depth retrieved from the sun photometer. The graph shows that the extinction from the lidar is systematically overestimated by about 30%. The lidar-related uncertainties propagate onto the aerosol concentration estimates. Equation (5) incorporates all the uncertainties related with other measurements and data processing. A proper uncertainty or sensitivity study would require an extensive research going well beyond the scope of this study.

ACPD
9, 6827–6854, 2009

Another limitation of the measurements to consider is that the lidar takes measurements directly above the roads. The cars are not only the source of fine aerosols due to gas burning but are also a separate source of mechanical mixing of the road dust that is lofted high above the roadways. Scanning lidar measurements in urban areas show dramatically increased particulate concentrations above major thoroughfares (e.g. Eichinger et al., 1993). This may explain why the lidar values of concentrations from the MEE calculations are systematically higher than the ground measurements such as RAMA, whose stations are located in some distance from the major roadways. This brings an important conclusion that a better and more representative particulate transect of the city would be obtained by using minor roads to cross the city.

From the theoretical point of view, the MEE is based on an entirely correct physical approach. Although the results contain uncertainties, the data set can be beneficial for any large scale aerosol data modelling. We think that the strengths of the MEE combined with lidar data outweigh the limitations of this approach and open totally new lidar capabilities for the community.

4.5 Comparison to RAMA data

Despite the resulting uncertainties contained within Eq. (5), the total aerosol concentration estimates are in general agreement with RAMA PM_{10} concentrations retrieved from the monitoring sites located near the lidar path. Figure 8 shows hour-average PM_{10} concentrations with values between 100 and 250 $\mu g/m^3$ for the times between 6 a.m. and 12 p.m. Because these are 1 h average, one can assume that there were events of much higher concentrations, such as the one observed instantaneously by the lidar at around 7 a.m. or presented in the histogram in Fig. 7 (red, urban). The discrepancies between the RAMA measurements and the lidar have several potential reasons. The major reason is the fact that RAMA reports only particles smaller than 10 microns while bigger particles are not uncommon in dusty environment of Mexico City. The lidar MEE retrieved concentrations show the total loading with no distinction between fine and coarse particles.

ACPD
9, 6827–6854, 2009

5 Conclusions

The results demonstrate the vertical structure of aerosols over Mexico City basin and its impact on a local scale. The ground surface pollution can reach as high as 1500 m above the ground. The high levels of aerosols associated with heavy traffic (and traffic jams) events indicate that the transportation system in Mexico City plays an important role in facilitating aerosol loadings in the city basin boundary layer.

The total aerosol mass concentration base levels in the basin are on the order of 200 $\mu g/m^3$ with small scale events peaking at as high as 900 $\mu g/m^3$. The concentrations outside of the basin (on the southern side of the rim) are about half of what was observed within the basin with base values of 100 $\mu g/m^3$. The vertical mixing outside of the basin is much more evident, with mixing depth as high as 2000 m above the ground. The residual layer is distinctly separated from the ground-based mixing.

The lidar inversion algorithm seems to overestimate the extinction coefficients which are systematically higher than the total extinction observed by the sun photometer. Nevertheless the total aerosol levels have a similar order of magnitude as the observations of PM_{10} from the RAMA network.

In the future, the quantitative estimation of the total aerosol loads from the mobile lidar can be improved by having a continuous measurement of size distribution along the measurement route. Also using secondary roads for transects could reduce the effect of the major thoroughfares, which can greatly set off the overall aerosol contributions from the urban areas.

References

Adachi, K. and Buseck, P. R.: Internally mixed soot, sulfates, and organic matter in aerosol particles from Mexico City, Atmos. Chem. Phys., 8, 6469–6481, 2008, http://www.atmos-chem-phys.net/8/6469/2008/.

Cooper, D. and Eichinger, W.: Structure of the atmosphere in an urban planetary boundary

layer from lidar and radiosonde observations, J. Geophys. Res., 99(D11), 22 937–22 948, 1994.
Cooper, D. I., Leclerc, M. Y., Archuleta, J., Coulter, R., Eichinger, E. W., Kao, C. Y. J., and Nappo, C. J.: Mass Exchange in the Stable Boundary Layer by Coherent Structures, Special Issue "Tribute to Marv Wesely", Agricultural and Forest Meteorology, 136, 114–131, 2006.
CAM: Programa para Mejorar la Calidad del Aire en el Valle de México 2002–2010, Comisión Ambiental Metropolitana, Mexico, 2002.
CAM: Inventario de emisiones de la atmósfera, Zona Metropolitana del Valle de México 2004, Comisión Ambiental Metropolitana, Mexico, 2006.
DeCarlo, P. F., Dunlea, E. J., Kimmel, J. R., Aiken, A. C., Sueper, D., Crounse, J., Wennberg, P. O., Emmons, L., Shinozuka, Y., Clarke, A., Zhou, J., Tomlinson, J., Collins, D. R., Knapp, D., Weinheimer, A. J., Montzka, D. D., Campos, T., and Jimenez, J. L.: Fast airborne aerosol size and chemistry measurements above Mexico City and Central Mexico during the MILAGRO campaign, Atmos. Chem. Phys., 8, 4027–4048, 2008, http://www.atmos-chem-phys.net/8/4027/2008/.
de Foy, B., Fast, J. D., Paech, S. J., Phillips, D., Walters, J. T., Coulter, R. L., Martin, T. J., Pekour, M. S., Shaw, W. J., Kastendeuch, P. P., Marley, N. A., Retama, A., and Molina, L. T.: Basin-scale wind transport during the MILAGRO field campaign and comparison to climatology using cluster analysis, Atmos. Chem. Phys., 8, 1209–1224, 2008, http://www.atmos-chem-phys.net/8/1209/2008/.
Del Gusta, M. and Marini, S.: On the retrieval of urban mass concentrations by a 532 and 1064 nm LIDAR, J. Aerosol Sci., 31(12), 1469–1488, 2000.
Di Girolamo, P., Ambrico, P. F., Amodeo, A., Boselli, A., Pappalardo, G., Spinelli, N.: Aerosol observations by lidar in the nocturnal boundary layer, Appl. Opt., 38, 4585–4595, 1999.
Doran, J. C., Fast, J. D., Barnard, J. C., Laskin, A., Desyaterik, Y., and Gilles, M. K.: Applications of lagrangian dispersion modeling to the analysis of changes in the specific absorption of elemental carbon, Atmos. Chem. Phys., 8, 1377–1389, 2008, http://www.atmos-chem-phys.net/8/1377/2008/.
Eichinger, W. E., Holder, H. E., Cooper, D. I., Hipps, L. E., Knight, R., Kustas, W. P., Nichols, J., and Prueger, J. H.: Lidar measurement of boundary layer evolution to determine sensible heat fluxes, J. Hydrometeorol., 6(6), 840–853, 2005.
Eichinger, W. E., Cooper, D. I., Hatfield, J., Hipps, L., Nichols, J. J., Pfeiffer, R., and Prueger, J. H.: Use of elastic lidar to examine the dynamics of plume dispersion from an agricultural

facility, Atmos. Environ., submitted, 2008a.
Eichinger, W., Eichinger, H., Cooper, D., Kreiger, J., and Carlson, E.: Lidar observations of high altitude activity associated with intermittent turbulence in a stable atmosphere, Bound. Lay. Meteorol., submitted, 2008b.
Eichinger, W. and Kraye, H.: The use of lidar to evaluate existing incident managment system on I-80 in Morris, Essex, and Passaic Counties in Northern New Jersey, Report No. 980004-7290, New Jersey Department of Transportation, 1998.
Eichinger, W., Buttler, W., Lebeda, C., Cooper, D., and Moses, J.: Barcelona air quality initiative, Alliance for Transportation Research, Project Document ATR 94-1, 1994.
Eichinger, W., Cooper, D., Buttler, W., Cottingame, W., and Tellier, L.: The use of lidar for the evaluation of traffic-related urban pollution, P. Soc. Photo-Opt. Inst., 2102, Bellingham, WA, 1993.
Eichinger, W., Cooper, D., Cottingame, W., Forman, P., Griegos, J., Osborn, M., Richter, D., Tellier, L., and Thornton, R.: The development of Raman water-vapor and elastic aerosol lidars for the Central Equatorial Pacific Experiment, J. Atmos. Ocean. Tech., 16(11), 1753–1766, 1999.
Fast, J. D., de Foy, B., Acevedo Rosas, F., Caetano, E., Carmichael, G., Emmons, L., McKenna, D., Mena, M., Skamarock, W., Tie, X., Coulter, R. L., Barnard, J. C., Wiedinmyer, C., and Madronich, S.: A meteorological overview of the MILAGRO field campaigns, Atmos. Chem. Phys., 7, 2233–2257, 2007, http://www.atmos-chem-phys.net/7/2233/2007/.
Holmen, B., Eichinger, W., and Flocchini, R.: Application of elastic lidar to PM_{10} emissions from agricultural non-point sources, Environ. Sci. Technol., 32(20), 3068–3076, 1998.
Holben, B. N., Eck, T. F., Slutsker, I., Tanré, D., Buis, J. P., Setzer, A., Vermote, E., Reagan, J. A., Kaufman, Y. J., Nakajima, T., Lavenu, F., Jankowiak, I., and Smirnov, A.: AERONET: a federated instrument network and data archive for aerosol characterization, Remote Sens. Environ., 66, 1–16, 1998.
Husar, R. B. and Falke, S. R.: The relationship between aerosol light scattering and fine mass, Center for Air Pollution Impact and Trend Analysis (CAPITA) Report, http://capita.wustl.edu/CAPITA/CapitaReports/BScatFMRelation/BSCATFM.HTML, 1996.
Klett, J. D.: Stable analytical inversion solution for processing lidar returns, Appl. Opt., 20, 211–220, 1981.
Klett, J. D.: Lidar inversion with variable backscatter/extinction ratios, Appl. Opt., 24, 1638–

1643, 1985.
Kovalev, V. A. and Eichinger, W. E.: Elastic Lidar: Theory, Practice and Analysis Methods, Wiley and Sons, New York, 2004.
Kovalev, V. A.: Lidar measurement of the vertical aerosol extinction profiles with range dependent backscatter-to-extinction ratios, Appl. Opt., 32, 6053–6065, 1993.
Kovalev, V. A.: Sensitivity of the lidar equation solution to errors in the aerosol backscatter-to-extinction ratio: influence of a monotonic change in the aerosol extinction coefficient, Appl. Opt., 34, 3457–3462, 1995.
Kovalev, V. A.: Stable near-end solution of the lidar equation for clear atmospheres, Appl. Opt., 42, 585–591, 2003.
Lagrosas, N. et al.: Correlation study between suspended particulate matter and portable automated lidar data, J. Aerosol Sci., 36, 439–454, 2005.
Mena-Carrasco, M., Carmichael, G. R., Campbell, J. E., Zimmerman, D., Tang, Y., Adhikary, B., D'allura, A., Molina, L. T., Zavala, M., García, A., Flocke, F., Campos, T., Weinheimer, A. J., Shetter, R., Apel, E., Montzka, D. D., Knapp, D. J., and Zheng, W.: Assessing the regional impacts of Mexico City emissions on air quality and chemistry, Atmos. Chem. Phys. Discuss., 8, 20283–20309, 2008, http://www.atmos-chem-phys-discuss.net/8/20283/2008/.
Molina, L. T., Kolb, C. E., de Foy, B., Lamb, B. K., Brune, W. H., Jimenez, J. L., Ramos-Villegas, R., Sarmiento, J., Paramo-Figueroa, V. H., Cardenas, B., Gutierrez-Avedoy, V., and Molina, M. J.: Air quality in North America's most populous city – overview of the MCMA-2003 campaign, Atmos. Chem. Phys., 7, 2447–2473, 2007, http://www.atmos-chem-phys.net/7/2447/2007/.
Molina, L. T., Madronich, S., Gaffney, J. S., and Singh, H. B.: Overview of MILAGRO/INTEX-B Campaign, IGAC Newsletter, Issue No. 38, 2–15, April 2008.
Nakajima T., Tonna G., Rao, R. Z., et al.: Use of sky brightness measurements from ground for remote sensing of particulate polydispersions, Appl. Opt., 35(15), 2672–2686, 1996.
Nunnermacker, L. J., Weinstein-Lloyd, J. B., Hillery, B., Giebel, B., Kleinman, L. I., Springston, S. R., Daum, P. H., Gaffney, J., Marley, N., and Huey, G.: Aircraft and ground-based measurements of hydroperoxides during the 2006 MILAGRO field campaign, Atmos. Chem. Phys., 8, 7619–7636, 2008, http://www.atmos-chem-phys.net/8/7619/2008/.
Shaw, W. J., Pekour, M. S., Coulter, R. L., Martin, T. J., and Walters, J. T.: The daytime mixing

layer observed by radiosonde, profiler, and lidar during MILAGRO, Atmos. Chem. Phys. Discuss., 7, 15025–15065, 2007, http://www.atmos-chem-phys-discuss.net/7/15025/2007/.

Shon, Z.-H., Madronich, S., Song, S.-K., Flocke, F. M., Knapp, D. J., Anderson, R. S., Shetter, R. E., Cantrell, C. A., Hall, S. R., and Tie, X.: Characteristics of the NO-NO_2-O_3 system in different chemical regimes during the MIRAGE-Mex field campaign, Atmos. Chem. Phys., 8, 7153–7164, 2008, http://www.atmos-chem-phys.net/8/7153/2008/.

Stephens, S., Madronich, S., Wu, F., Olson, J. B., Ramos, R., Retama, A., and Muñoz, R.: Weekly patterns of México City's surface concentrations of CO, NO_x, PM_{10} and O_3 during 1986–2007, Atmos. Chem. Phys., 8, 5313–5325, 2008, http://www.atmos-chem-phys.net/8/5313/2008/.

Stone, E. A., Snyder, D. C., Sheesley, R. J., Sullivan, A. P., Weber, R. J., and Schauer, J. J.: Source apportionment of fine organic aerosol in Mexico City during the MILAGRO experiment 2006, Atmos. Chem. Phys., 8, 1249–1259, 2008, http://www.atmos-chem-phys.net/8/1249/2008/.

Talbot, R., Mao, H., Scheuer, E., Dibb, J., Avery, M., Browell, E., Sachse, G., Vay, S., Blake, D., Huey, G., and Fuelberg, H.: Factors influencing the large-scale distribution of Hg° in the Mexico City area and over the North Pacific, Atmos. Chem. Phys., 8, 2103–2114, 2008, http://www.atmos-chem-phys.net/8/2103/2008/.

Thornhill, D. A., de Foy, B., Herndon, S. C., Onasch, T. B., Wood, E. C., Zavala, M., Molina, L. T., Gaffney, J. S., Marley, N. A., and Marr, L. C.: Spatial and temporal variability of particulate polycyclic aromatic hydrocarbons in Mexico City, Atmos. Chem. Phys., 8, 3093–3105, 2008, http://www.atmos-chem-phys.net/8/3093/2008/.

Zheng, J., Zhang, R., Fortner, E. C., Volkamer, R. M., Molina, L., Aiken, A. C., Jimenez, J. L., Gaeggeler, K., Dommen, J., Dusanter, S., Stevens, P. S., and Tie, X.: Measurements of HNO_3 and N_2O_5 using ion drift-chemical ionization mass spectrometry during the MILAGRO/MCMA-2006 campaign, Atmos. Chem. Phys., 8, 6823–6838, 2008, http://www.atmos-chem-phys.net/8/6823/2008/.

Fig. 1. The University of Iowa mobile vertical lidar (1064 nm 50 Hz 25 mJ/pulse laser, 100 MHz digitizer, 1.5 m spatial and 1 s temporal resolution) during the MILAGRO 2006 campaign.

ACPD

9, 6827–6854, 2009

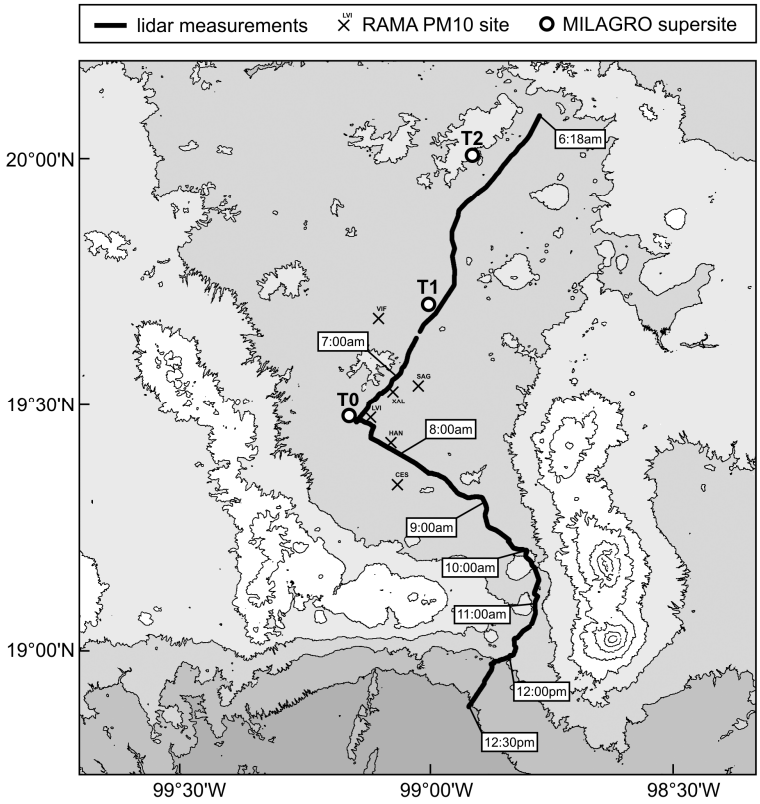

Fig. 2. The Mexico City basin. Black line indicates mobile lidar trajectory with time marks on 7 March 2006. Crosses show selected RAMA PM_{10} sites and circles indicate MILAGRO supersites T0, T1 and T2.

ACPD
9, 6827–6854, 2009

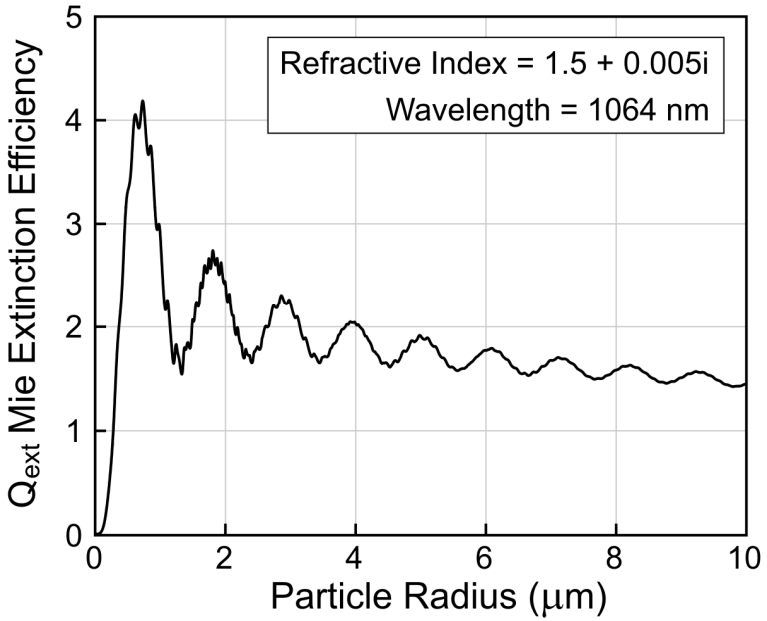

Fig. 3. Q_{ext} Mie extinction efficiency used for MEE calculations.

ACPD
9, 6827–6854, 2009

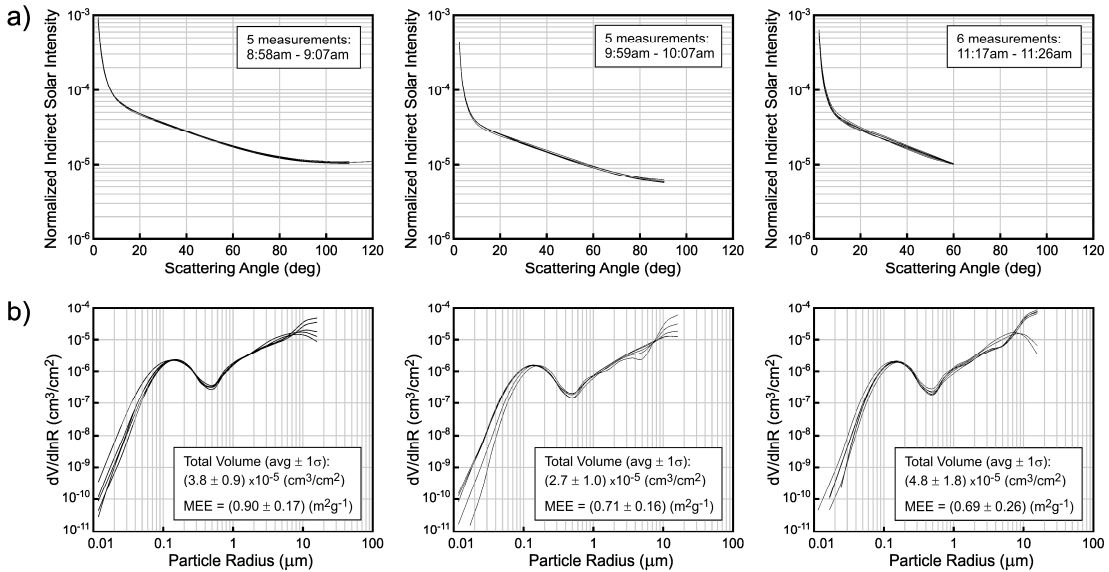

Fig. 4. (a) Sun photometer raw data (showing 500 nm only) recorded in Mexico City on 7 March 2006. **(b)** Corresponding aerosol size distributions (ASD) retrieved from sun photometer measurements using SKYRAD.pack.v.4.2 inversion code. The inset shows total volume and MEE values.

ACPD
9, 6827–6854, 2009

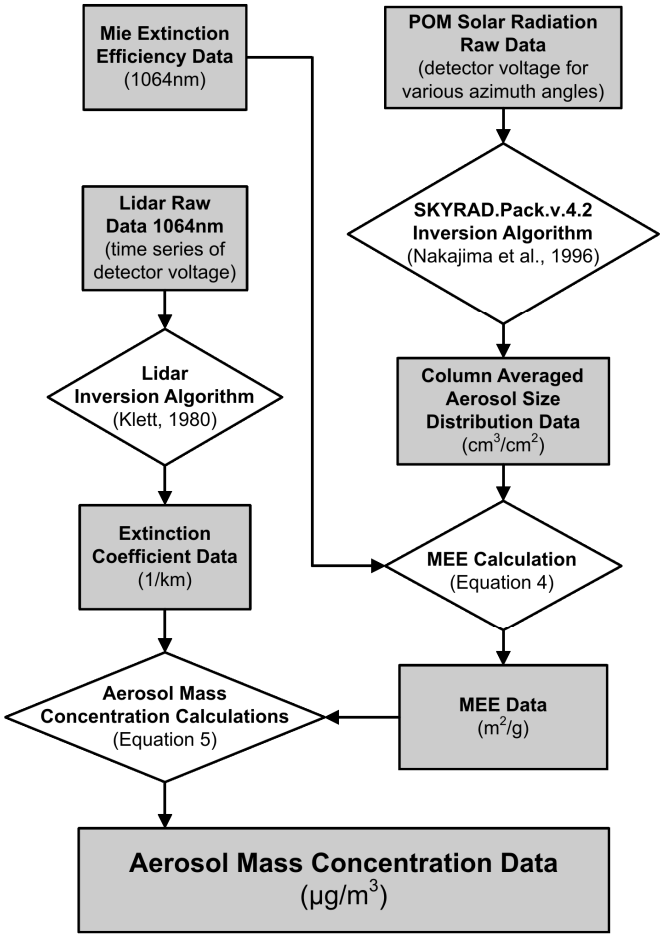

Fig. 5. Lidar to aerosol mass concentration data processing flowchart.

ACPD
9, 6827–6854, 2009

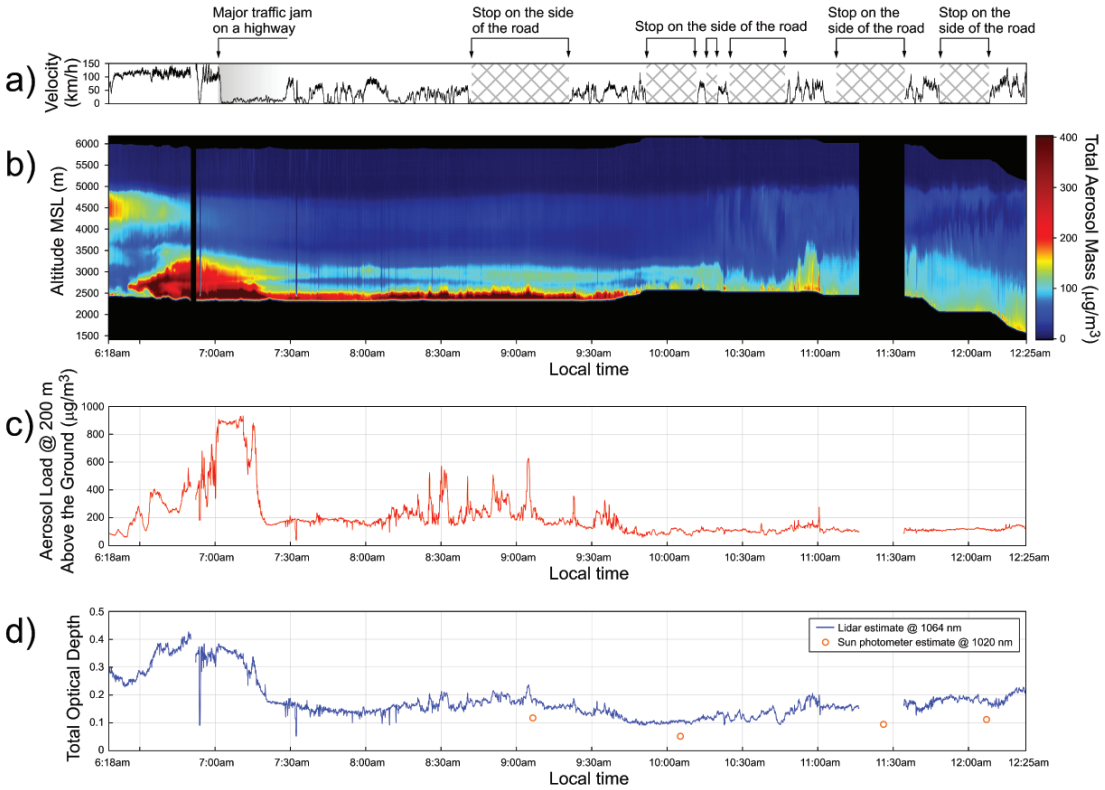

Fig. 6. Lidar vertical profiles of aerosol loadings over Mexico City on 7 March 2006: **(a)** lidar velocity over ground, indicating periods of heavy traffic and several stops, **(b)** color coded total aerosol vertical concentrations in Mexico City basin, **(c)** concentration levels at 200 m above the ground, **(d)** total optical depth calculated from lidar data (blue line) and from sun photometer (orange cirles).

ACPD
9, 6827–6854, 2009

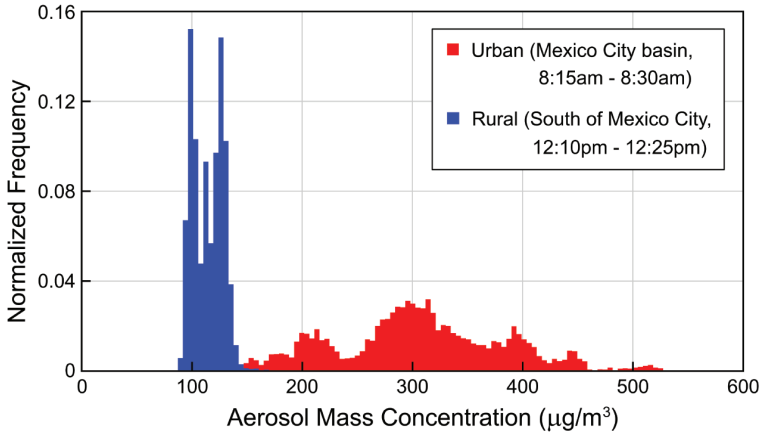

Fig. 7. Histogram of aerosol mass concentration values observed at 200 m above the ground in a 15 min time-span, inside the city basin (red) and outside the basin blue.

ACPD
9, 6827–6854, 2009

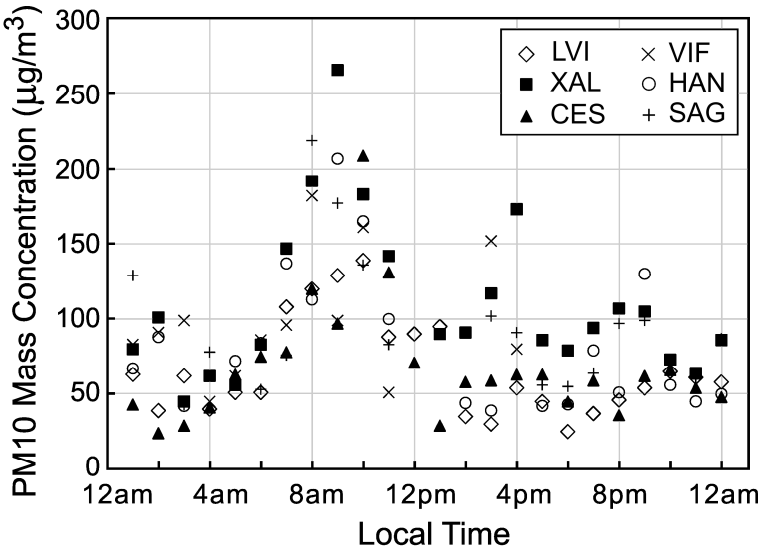

Fig. 8. Time series of PM_{10} concentrations on 7 March 2006, for selected RAMA ground monitoring sites.

ACPD
9, 6827–6854, 2009

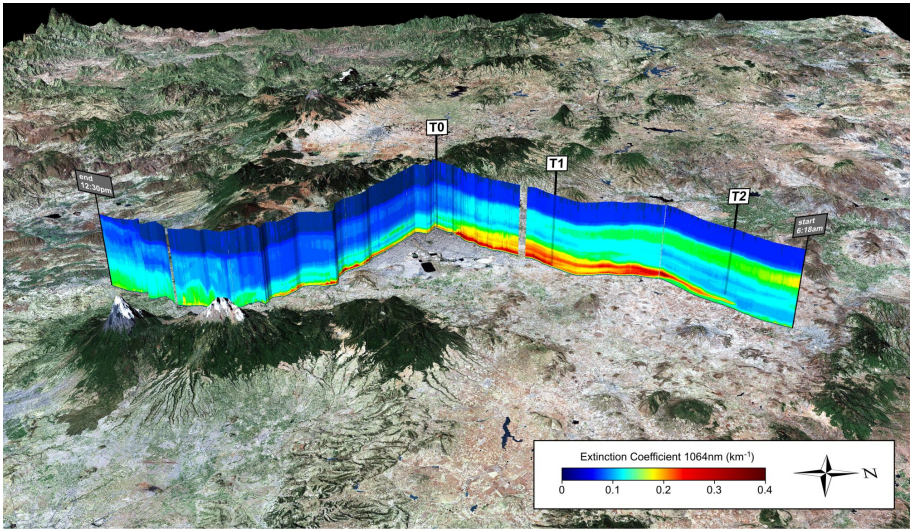

Fig. 9. The lidar color coded vertical distribution of aerosols over Mexico City basin on 7 March 2006, looking West. The dark red indicates heavy aerosol loading and dark blue indicate clean air in the free troposphere. The transect presents a stable layering within the valley and an intensive vertical mixing outside of the basin. (Elevation model and satellite imaging source: USGS).

ACPD
9, 6827–6854, 2009